Electron-stimulated desorption of D^+ from D_2O ice: Surface structure and electronic excitations

M. T. Sieger, W. C. Simpson, and T. M. Orlando*
Environmental Molecular Sciences Laboratory, Pacific Northwest National Laboratory, P.O. Box 999, MSIN K-14, Richland, Washington 99352
(Received 12 December 1996)

We present a study of the electron-stimulated desorption of deuterium cations (D^+) from thin (1–40 ML) D_2O ice films vapor deposited on a Pt(111) substrate. Measurements of the total yield and velocity distributions as a function of temperature from 90 to 200 K show that the D^+ yield changes with film thickness, surface temperature, and ice phase. We observe two energy thresholds for cation emission, near 25 and 40 eV, which are weakly dependent upon the ice temperature and phase. The cation time-of-flight (TOF) distribution is at least bimodal, indicating multiple desorption channels. A decomposition of the TOF distributions into ''fast'' and ''slow'' channels shows structure as a function of excitation energy, film thickness, and temperature. The D^+ yield generally increases with temperature, rising near 120 K on amorphous ice, and near 135 K on crystalline ice. The amorphous-crystalline phase transition at $\sim$160 K causes a drop in total desorption yield. The temperature dependence of D^- desorption via the $^2B_1$ dissociative electron attachment resonance is very similar to the slow D^+ yield, and likely involves similar restructuring and lifetime effects. The data collectively suggest that a thermally activated reduction of surface hydrogen bonding increases the lifetime of the excited states responsible for ion desorption, and that these lifetime effects are strongest for excited states involving a_1 bands [S0163-1829(97)05931-6]

I. INTRODUCTION

The behavior of water and ice under energetic particle bombardment is a topic of great interest for many disciplines including astrophysics,[1] and radiation biology.[2] It is also an important consideration in the treatment and storage of radioactive wastes, which are often in wet environments. Most studies of ice radiolysis have focused upon the fragmentation and desorption caused by the interaction of highly energetic particles ($E>1$ keV) with the bulk.[1,3] High-energy collisions in a solid, however, also create vast numbers of secondary electrons with energies in the 1–100-eV range.[4] The interaction of these low-energy electrons with ice plays a key role in its radiolytic decomposition, because these secondaries have energies resonant with valence excitations, which can lead to bond breaking and ejection of atoms and molecules from the solid. Though the importance of electronic excitations in sputtering and stimulated desorption from ice is well recognized,[1,3,5] the detailed physics of this process is not fully understood. It is therefore of interest to examine the stimulated desorption of molecules, ions, and neutral fragments from amorphous water ice, which is often used as a model of the liquid state,[6] and its crystalline polymorph. Close examination of stimulated desorption from nanoscale ice films can also yield clues about the structure of water/solid interfaces.[7]

The bulk and surface properties of water and ice have been investigated with a wide variety of probes, including photoemission,[7–13] infrared spectroscopy,[6,8,14,15] electron diffraction,[16,17] x-ray diffraction,[6,18,19] thermal desorption,[20–25] electron-energy-loss spectroscopy,[26] optical absorption,[27] and scanning tunneling microscopy.[28] Theoretical efforts include calculations of the electronic, bulk, and surface structures of ice.[15,29–31] Many reviews of the general properties of water, ice, and ice films are in the literature.[6,7,32] Despite the tremendous amount of work performed in this field, the nature of the ice surface is still a topic of active investigation.

Electron-stimulated desorption (ESD) and photon-stimulated desorption (PSD) are well-known techniques[7,33] which are very surface sensitive. Previous low-energy (5–150 eV) ESD and PSD studies of amorphous H_2O/D_2O ice surfaces have examined the stimulated production of H_2/D_2,[34] D and O,[5] H^-/D^-,[35,36] and H^+/D^+.[37–46] Some studies of H^+ ESD from H_2O ice reported a threshold near 20–25 eV and several desorption pathways, whose relative importance depended upon the excitation energy.[38,39] The excitations responsible for cation emission have been assigned to two-hole one-electron ($2h1e$) shake-up and two-hole ($2h$) configurations.[38–40] It has been postulated that these excitations are sensitive to the local environment of the water molecule.[40,41,45] None of these previous studies, however, examined the temperature and ice phase dependence of the cation emission.

In this paper, we present a detailed investigation of the ESD of deuterium cations (D^+) from thin (1–40 ML) amorphous and crystalline D_2O ice films deposited on a Pt(111) substrate. We have measured the total cation yield and time-of-flight (TOF) distributions as a function of incident electron energy, ice temperature, and film thickness. We find incident electron energy thresholds for cation emission near 25,40, and possibly 70 eV. The D^+ total yield changes significantly as the temperature is ramped from 90 to 200 K, and is different for amorphous and crystalline ice. A distinct drop in the total yield at about 160 K is coincident with the irreversible amorphous-crystalline phase transition. The D^+ TOF distributions can be roughly separated into ''fast'' and ''slow'' peaks. Decomposition of the velocity distributions into these components shows that these desorption channels have breakpoints at the same temperatures, but otherwise behave differently. The slow cation component has essentially the same temperature and ice thickness dependence

as the anion (D^-) yield, produced via the $^2B_1$ dissociative electron attachment resonance,[36] whereas the fast cation yield closely follows changes in the work function with temperature.[8] The data are consistent with a thermally activated reduction in surface hydrogen bonding, and reorientation or rearrangement of the surface molecules. Examination of the relevant dissociative states of the water molecule suggest that the lifetimes of excited states are affected by these changes in the surface hydrogen bonding.

II. EXPERIMENT

The experiments were performed in an ultrahigh-vacuum chamber (base pressure 2×10^{-10} Torr) equipped with a pulsed low-energy electron gun, a quadrupole mass spectrometer (QMS), an effusive D_2O gas doser, and a time-of-flight (TOF) spectrometer. The Pt(111) substrate was mounted in thermal contact with a liquid-nitrogen reservoir, and was radiatively heated by a tungsten filament. The substrate temperature was monitored with a thermocouple spot welded to the substrate. A computer-controlled feedback system drove the temperature ramp, which was 8 K/min for both temperature-programmed desorption (TPD) and D^+ flux vs temperature measurements. The samples were prepared by depositing thin (1–40 ML) films of D_2O ice at a rate of 4–8 ML/min, with the film thickness of the amorphous samples calibrated by comparing TPD spectra with previously published results.[23,24] (See note added in proof.) Coverages are reported in monolayers of ice, where 1 ML is defined as the number of water molecules in a complete bilayer of the (111) face of cubic ice ($\sim10^{15}$ molecules/cm^2). The electron beam has a typical current density of 10^{14} electrons/cm^2/s (continuous beam), and a beam spot size of ~1.5 mm^2. The electron beam was pulsed at 200 Hz, with a pulse width of 700 ns, giving an effective electron dose of about 10^{10} electrons/cm^2/s, or 10^{-5} electron/surface D_2O molecule/s. The incident electron energy (E_i) could be varied continuously from 5 to 100 eV, with an energy spread of ~0.3 eV. Both the electron beam incident angle and TOF entrance grid were 45° with respect to the surface normal. Since the cation desorption angle relative to the surface normal can change with temperature,[47] a 75-V extraction pulse was applied to the TOF grid following the incident electron pulse. An investigation of the collection efficiency versus extraction voltage indicated that an extraction field greater than 50 V was sufficient to collect all desorbing cations. Due to the use of this extraction field, our TOF signal does not represent a true velocity distribution, but instead measures the time of arrival. The TOF has unit mass resolution, and the primary cation observed was D^+, with a small H^+ signal due to H_2O and HDO. The H^+ TOF peak was well separated from the D^+ peak, and does not contribute to any of the reported data. The total ion yield was measured by integrating the area under the D^+ TOF signal.

In the course of these experiments, it was noted that the width of the D^+ TOF distribution increased with incident electron flux. Above an electron pulse frequency of 200 Hz, corresponding to electron fluxes of $>10^{10}$ electrons/cm^2/s, the D^+ TOF peak began to broaden noticeably, which we attributed to surface charging. To minimize such charging effects, our data were acquired at 200 Hz. This incident electron flux is, to our knowledge, more than 100 times lower than those used in previous studies.

Of the many known polymorphs of ice, only four play an important role in the temperature and pressure environment of our experiments: two forms of amorphous ice and two crystalline phases. It is possible to prepare each of these polymorphs by controlling the deposition temperature and annealing history. D_2O condensation at temperatures below 100 K forms microporous amorphous ice,[20–22,31,48] which is characterized by a high surface area and low density. Sintering microporous ice between 100 and 120 K or depositing at temperatures between 110 and 130 K generates normal (nonporous) amorphous ice. Films grown above 140 K form either hexagonal crystalline ice $Ih(0001)$ or cubic crystalline ice $Ic(001)$,[16,17] which we will refer to as simply crystalline ice. The difference between ice Ih and Ic lies in the bilayer stacking sequence, and our surface-sensitive ESD measurements cannot distinguish between the two. Amorphous ice annealed at 162 K undergoes a phase transition to polycrystalline ice.[24,25] In vacuum, D_2O ice evaporates rapidly above 165 K, as shown by temperature-programmed desorption.[20,22–25] Our investigations focused on the nonporous amorphous and crystalline polymorphs. Amorphous samples were prepared by depositing D_2O vapor on the Pt(111) substrate at 110 K, and crystalline samples were prepared by condensation at 155 K. Following deposition, the samples were annealed at their respective growth temperatures until the background D_2O pressure fell below 10^{-9} torr (2–3 min), and were then cooled to 90 K for measurement. The desorption rate of crystalline ice is not negligible at 155 K, and, as a consequence, the crystalline films examined here may be somewhat thinner than 40 ML.

III. RESULTS

In Sec. III A, we present the threshold and electron energy dependence of the D^+ ESD total yield and time-of-flight data. In Secs. III B and III C, we present the temperature and thickness dependence of the total yield and velocity-resolved TOF data, respectively. In Sec. III D, we compare the yield of D^- (produced via the $^2B_1$ dissociative electron attachment resonance) and work-function data with the velocity-resolved D^+ yields.

A. Thresholds and electron energy dependence

1. Total yield

Figures 1(a) and 1(b) show the total D^+ ESD yields as a function of E_i from thick (40 ML) amorphous and crystalline D_2O ice films, respectively, at two representative temperatures. The spectra are offset for clarity. Two major thresholds are evident, denoted A ($\sim$22–24 eV) and B ($\sim$40 eV). Our results are in agreement with earlier measurements,[38–44] which observed an onset at 20–21 eV and a rapid rise at 24–25 eV for proton ESD and PSD from amorphous H_2O ice. Threshold A has been assigned to deep valence excitation followed by shake-up to two-hole–one-electron ($2h1e$) dissociative excited states.[38–40] Threshold B has been observed in PSD measurements,[43] and was tentatively assigned to valence excitation plus shakeoff to form two-hole ($2h$) states which dissociate via a Coulomb explosion.[40,43,49]

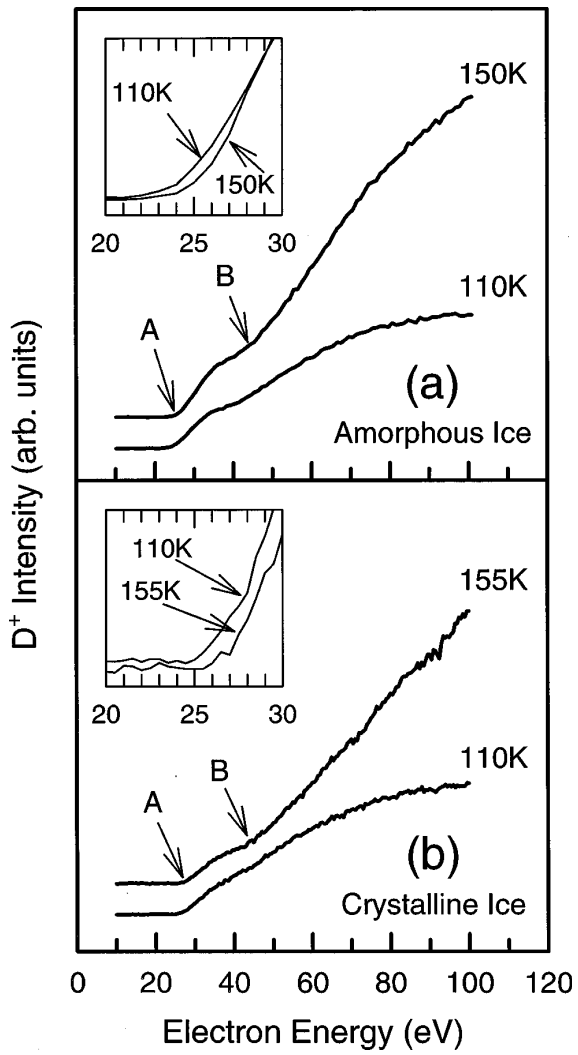

FIG. 1. Total D^+ ESD yield vs incident electron energy (E_i) at representative temperatures from 40 ML films of (a) amorphous ice, and (b) crystalline ice. The curves are offset for clarity. Primary and secondary thresholds are labeled *A* and *B*. Insets show near-threshold behavior as a function of temperature.

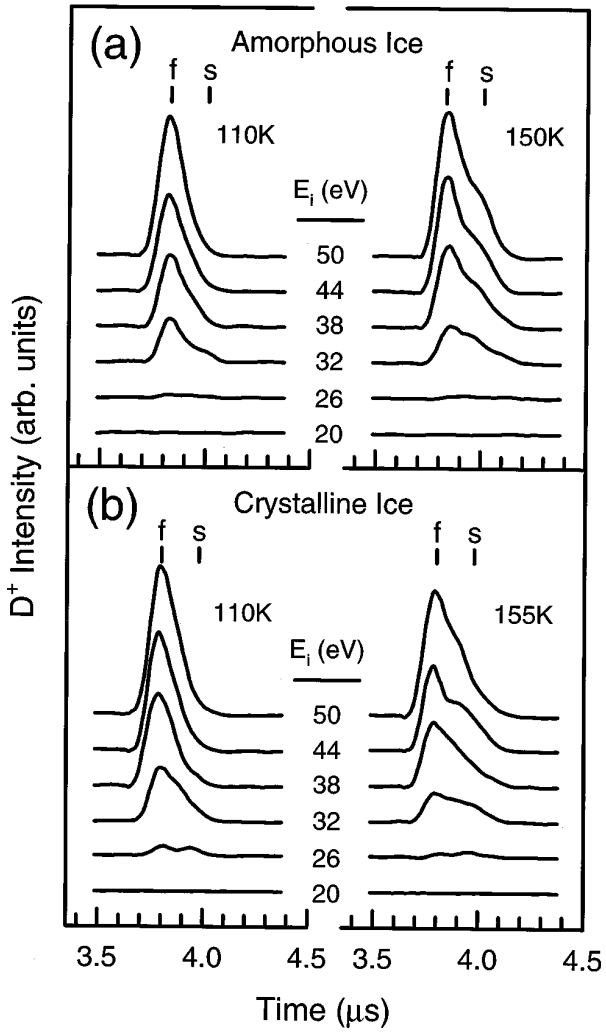

FIG. 2. D^+ time-of-flight distributions from (a) amorphous ice, and (b) crystalline ice, at selected incident electron energies (E_i) and substrate temperatures. The peak height sampling times t_{fast} (f) and t_{slow} (s) are indicated by vertical lines. The data have been smoothed for display.

The insets show the onset of emission at low and high temperatures. The onset for desorption from crystalline ice appears to shift by almost +2 eV between 110 and 155 K, while the amorphous ice shows a smaller shift. This shift in threshold energy cannot be accounted for by the temperature dependence of the work function.[8] Instead, it appears that an excitation channel is being suppressed for high-temperature crystalline ice. Above threshold, the yield increases rapidly with increasing excitation energy until about 70 eV, where the slope decreases. PSD measurements have also noted a decrease in yield at higher excitation energies.[43] Rough estimates of the incident electron flux and the total D^+ flux at the detector give a quantum yield of 10^{-2}–10^{-3} D^+/electron at $E_i = 100$ eV at $T = 155$ K for crystalline ice, and about half that at $T = 110$ K. The quantum yield is similar for amorphous ice. At excitation energies above 40 eV, the yield is strongly temperature dependent, and generally increases with temperature for both amorphous and crystalline ice. Below 40 eV, the yield changes only weakly with temperature (except for the threshold shift mentioned above). Overall, there appear to be only superficial differences in the energy dependence of the deuteron yields between amorphous and crystalline ice, though the temperature dependence is different as discussed in Sec. III B.

2. TOF distributions

D^+ TOF distributions in the near-threshold region are shown in Figs. 2(a) and 2(b) for low and high temperatures from amorphous and crystalline ice. There do not appear to be any strong differences between the two phases, but the TOF line shapes do change considerably with temperature. At $T = 110$ K, only one peak is evident in the TOF spectrum. At $T = 150/155$ K, however, the distribution is bimodal, with a shoulder at longer times. The TOF line shape for our experimental geometry is not well characterized, and there appear to be several unresolved components in the distribution, so fitting the data to extract individual peak intensities is impractical. The detection geometry and the use of a strong extraction field also precludes transforming the data into absolute energy units. Previous studies[38,39] observed a bimodal

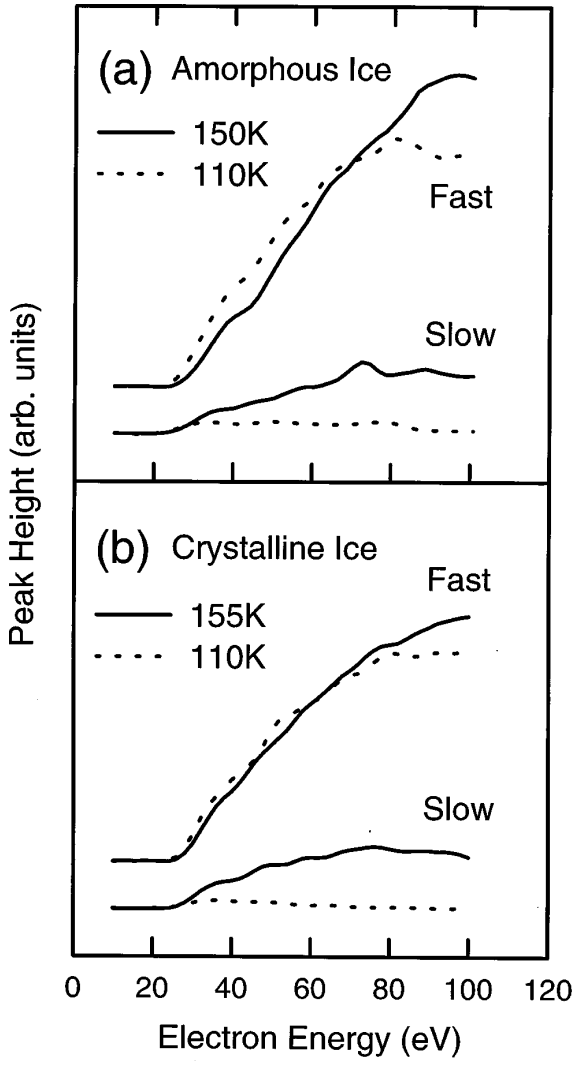

FIG. 3. Fast and slow D^+ time-of-flight peak heights as a function of incident electron energy (E_i) at low (dashed line) and high (solid line) substrate temperatures on (a) amorphous ice, and (b) crystalline ice.

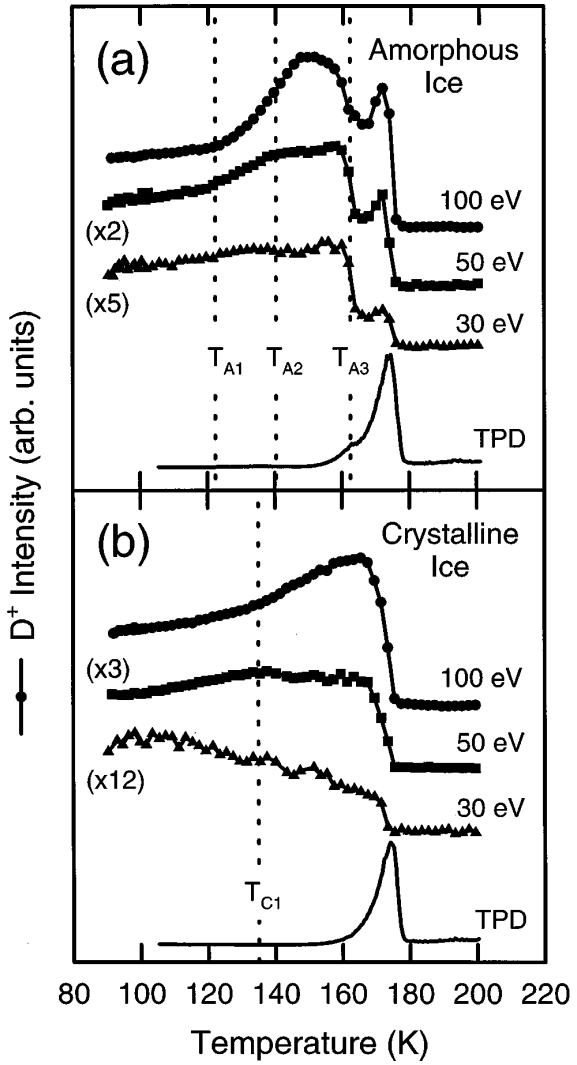

FIG. 4. Total D^+ ESD yield as a function of substrate temperature for selected incident electron energies, and a typical TPD spectrum showing film desorption rate for (a) amorphous ice, and (b) crystalline ice. Temperatures of interest are indicated by vertical dashed lines and labels. The temperature ramp was 8 K/min.

kinetic-energy distribution for H^+ ESD from ice, and reported kinetic energies of 3–4 and 6–10 eV for the ''slow'' and ''fast'' ion channels, respectively. We cannot verify these energies, but we can gain an estimate of how the fast and slow D^+ intensities change with excitation energy and temperature by recording the TOF peak height at two times t_{fast} and t_{slow}, indicated by short vertical lines labeled f and s in Fig. 2. We chose t_{fast} to coincide with the maximum of the distribution at low temperature (i.e., when the slow component is at a minimum), and t_{slow} to be on the slow shoulder at $t_{\text{fast}}+0.18$ μs. While small changes in t_{fast} and t_{slow} do affect the relative peak heights, the general features of the energy and temperature dependence do not change significantly. It was found that t_{fast} is independent of energy for $E_i<\sim 70$ eV. Electron energies higher than 70 eV produce slightly faster ions.

Shown in Figs. 3(a) and 3(b) are the fast and slow peak heights as a function of E_i for amorphous and crystalline ice, respectively. As with the total yields, the decomposition into fast and slow channels appears to be grossly similar for the two ice phases. The threshold energies for the fast and slow channels are the same, to within the accuracy of our measurements (± 1 eV). The emission of slow D^+ is the most sensitive to temperature, but does not change much with E_i. The fast D^+ signal decreases upon heating for $E_i<70$ eV, but increases for higher energies. Since the fast peak in the TOF distribution also shifts to shorter times for $E_i>70$ eV, it is possible that another desorption channel is active above 70 eV which produces extra fast deuterons. This channel is temperature dependent.

B. Temperature dependence

1. Total yield

Figure 4(a) is a plot of the total D^+ yield vs temperature from amorphous ice at selected excitation energies, and a corresponding D_2O TPD spectrum. The D_2O desorption rate is negligible below 150 K, and the film begins to desorb at about 155 K.[24] Amorphous ice has a higher vapor pressure than crystalline ice, and the dip in the TPD spectrum at 162 K is due to the amorphous-crystalline ($a-c$) phase transi-

tion, which has been well characterized in previous studies.[24,25] The desorption rate increases rapidly near 170 K, and the film has almost completely evaporated by 180 K. For the total D^+ yield measurements, the temperature was cycled from 90−140−90−200 K at a constant rate of 8 K/min. This cycle was used to determine the reversibility of the temperature dependence between 90 and 140 K. The D^+ yield as a function of temperature shows several features. The vertical dashed lines mark temperatures of interest, labeled T_{A1} (120–125 K), T_{A2} (140–145 K), and T_{A3} (160–165 K). The D^+ yield is roughly linear with temperature between 90 K and T_{A1}, and shows an increase between T_{A1} and T_{A2} which is dependent upon E_i. The increase in yield is roughly exponential, suggesting an activated process. We have chosen T_{A1} to coincide with a noticeable change in yield, and it should be noted that when we refer to the ''transition at T_{A1},'' we are referring to this activated process. The increase in yield between T_{A1} and T_{A2} is greater at higher excitation energies, and is reversible: the 90−140−90-K heating cycle has no effect on the observed temperature dependence in this range. The D^+ yield levels off between T_{A2} and T_{A3} for $E_i=30$ and 50 eV. The behavior near T_{A2} is not completely reversible: annealing the sample above T_{A2} apparently causes the $a-c$ transition to occur at temperatures below 160 K. The $a-c$ transition is marked by a steep drop in yield at T_{A3}, and is completely irreversible. The yield then increases sharply near 170 K as the film desorbs. The D^+ signal from water vapor above the surface is too small to be detected, so the increase in yield is presumably associated with the structure of the ice surface as it sublimes. The transition temperatures quoted here depend upon the heating rate,[20,24] so care should be exercised when comparing the results to other studies. (See note added in proof.) It is clear, however, that the amorphous ice undergoes transitions at $T_{A1}-T_{A2}$ and T_{A3} which change the cross section for deuteron desorption.

Figure 4(b) shows the temperature dependence of the D^+ yield from crystalline ice and a D_2O TPD spectrum. The magnitude of the yield is comparable to the yield from amorphous ice. However, the temperature dependence is very different, with only one breakpoint in the slope near 135 K (T_{C1}), which is most apparent at 50-eV excitation. Crystalline ice does not exhibit the $a-c$ phase transition, so the shoulder in the TPD spectrum and associated drop in the D^+ yield do not occur. The deuteron yield at $E_i=30$ eV decreases with increasing temperature, which may be related to the threshold shift to higher E_i upon heating [see Fig. 1(b) inset]. At $E_i=50$ eV, the yield rises up to T_{C1}, then levels off, and does not change much until the film evaporates. At 100 eV, however, the yield grows larger after T_{C1}. This T_{C1} transition, like T_{A1} in the amorphous ice, is reversible: heating in the 90−140−90-K temperature cycle shows no change in the yield.

2. TOF distributions

Changes in the total yield as a function of temperature, electron energy, and crystalline phase reflect changes in the dominant desorption channels. It is therefore important to examine the fast and slow ion components of the TOF distribution as a function of temperature and ice phase. In Fig. 5, the D^+ TOF distributions for $E_i=50$ eV are plotted as a function of temperature for amorphous and crystalline ice. The distributions for $E_i=30$ and 100 eV are similar to those for 50 eV. Both amorphous and crystalline ice show the emergence of a slow component at higher temperatures. We can extract the peak height at t_{fast} and t_{slow} in the same manner as for the threshold data, and examine in detail how the two components behave as a function of temperature.

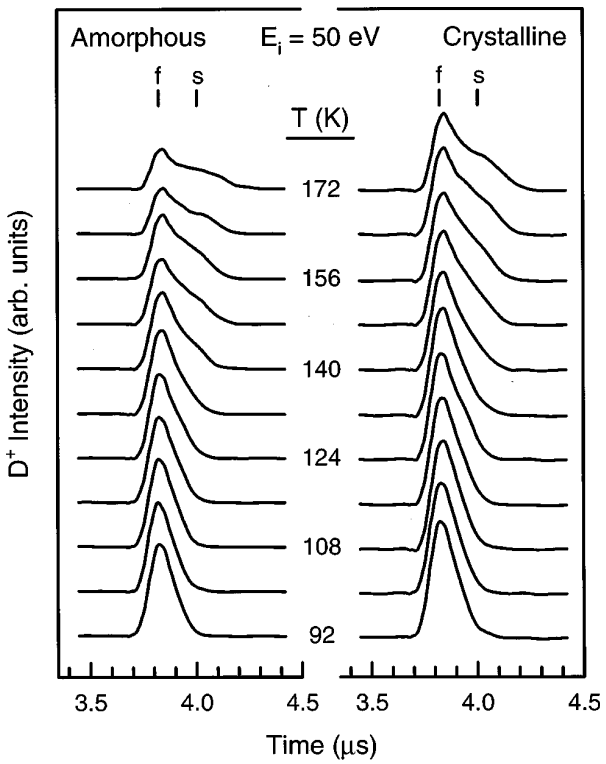

FIG. 5. D^+ time-of-flight distributions from amorphous and crystalline ice for $E_i=50$ eV at selected substrate temperatures. Note the appearance of slow deuteron emission at temperatures >120 K. The peak height sampling times t_{fast} (f) and t_{slow} (s) are indicated by vertical lines.

Figure 6(a) shows the temperature dependence of the fast and slow D^+ peak heights at $E_i=30$, 50, and 100 eV for amorphous ice. The data have been arbitrarily scaled for display. The similarity between the different excitation energies is striking, given the apparent dissimilarity of the total yields in Fig. 4. Both the fast and slow channels have breakpoints at about the same temperatures, and decrease at the $a-c$ phase transition. The temperature dependence of the slow channel is independent of E_i, and increases between T_{A1} and T_{A2}. The fast emission channel has the opposite behavior with temperature; it decreases between T_{A1} and T_{A2}, except for $E_i=100$ eV, where it *increases*. These data further support the idea than an extra desorption channel is active above 70 eV. The difference between the fast deuteron yields at 50 and 100 eV may be due to this extra channel. This extra desorption channel has the same temperature dependence as the slow product, suggesting that it is related to the slow D^+ channel.

The apparent dissimilarities in the temperature dependence of the total D^+ yield from amorphous ice at different E_i can then be explained in terms of the relative cross section for the fast and slow desorption channels. The total yield at $E_i=30$ eV is nearly independent of temperature; this is be-

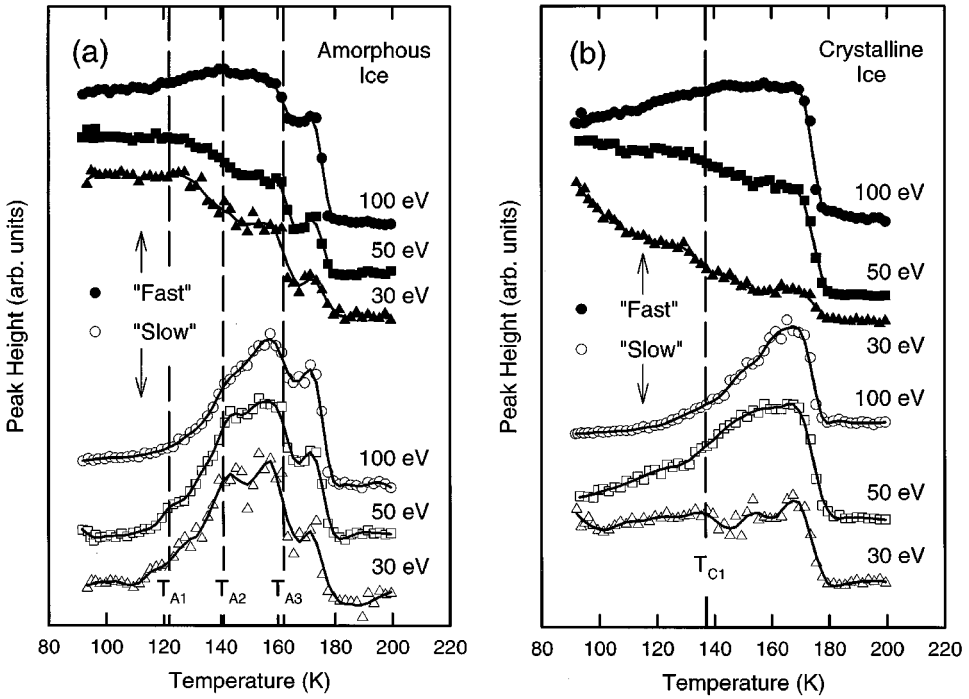

FIG. 6. Fast (filled symbols) and slow (empty symbols) D^+ time-of-flight peak heights at selected incident electron energies, as a function of temperature from (a) amorphous and (b) crystalline ice. Temperatures of interest are indicated by vertical dashed lines. The data have been arbitrarily scaled for display.

cause the increasing slow D^+ yield is the same magnitude as the decreasing fast D^+ yield, and the two contributions effectively cancel out. At 50 eV, the decrease in the fast channel does not entirely cancel out the increase in the slow channel, and when added together give a modest increase in total yield above T_{A1}. At 100 eV, the increase in fast *and* slow D^+ intensities collectively give a large increase in total yield.

Figure 6(b) shows the fast and slow D^+ peak heights for crystalline ice as a function of temperature. The overall temperature dependence is simpler than from amorphous ice, with the only strong change occurring near T_{C1}. The slow deuteron emission increases near T_{C1} for $E_i=50$ and 100 eV, but remains relatively constant for $E_i=30$ eV. The fast D^+ yield at 50 and 100 eV appears to be similar to the amorphous case. The 30-eV fast D^+ yield, however, decreases rapidly with temperature. The observed threshold shift with temperature [see Fig. 1(b)] could be a cause for the flat slow D^+ yield and the large drop in the fast D^+ yield at 30 eV. A decrease in the total desorption cross section with increasing temperature (due to the threshold shift) would counteract the increase in the slow D^+ intensity, and augment the decrease in the fast D^+ intensity at $E_i=30$ eV.

The fact that all desorption channels appear to have breakpoints at the same temperatures suggest that changes in the surface environment are occurring. Though these changes in the surface environment occur at different temperatures for amorphous and crystalline ice, they appear to have similar effects on the desorption. In general, the fast and slow deuteron channels have nearly the opposite temperature dependence, which suggests a population effect; i.e., the fast emitters begin to be converted into slow emitters at T_{A1} and T_{C1}. The surface environment which produces slow deuterons also can produce fast deuterons above $E_i=70$ eV. The common drop in intensity for the fast *and* slow D^+ at the $a-c$ phase transition suggests that all channels on the polycrystalline surface may have a smaller total excitation cross section, shorter excited-state lifetime, or perhaps a smaller number of active sites than the amorphous and single crystalline phases.

C. Thickness dependence

1. Total yield

The data presented in Figs. 1–6 were obtained on thick (~40 ML) ice layers. However, the total deuteron yield depends upon the thickness of the ice film, as shown in Fig. 7(a) and 7(b). The data in these figures were obtained during deposition. The yield from amorphous ice [Fig. 7(a)] rises very rapidly up to about 2-ML coverage, rises more slowly to a maximum, and then decreases to a saturation value around 25 ML. The thickness dependence is very different for crystalline ice [Fig. 7(b)]. The yield rises rapidly to 2 ML, the same as amorphous ice, but then decreases to a minimum at about 8 ML, and gradually rises to a near-saturation value by 40 ML. A similar behavior of the H^+-ion yield as a function of thickness was observed for H_2O/Ti(001) by Stockbauer *et al.*[44] The differences between the amorphous and crystalline thickness dependence may be due to different growth modes. It is surprising that such thick films are required to reach an equilibrium surface. It is known that amorphous ice forms clusters at low coverage on Pt(111).[8,28] These clusters coalesce at higher coverages, and our observations may be due to the change in cluster density as coverage increases. The surface roughness can also have an important impact on the D^+ yield, which is discussed in another publication.[50]

2. TOF distributions

The TOF distributions are also thickness dependent, as shown in Fig. 8 for $E_i=50$ eV. At 110 K, the slow shoulder is pronounced for the thin amorphous film, but decreases with film thickness and is not present for the thick film. The

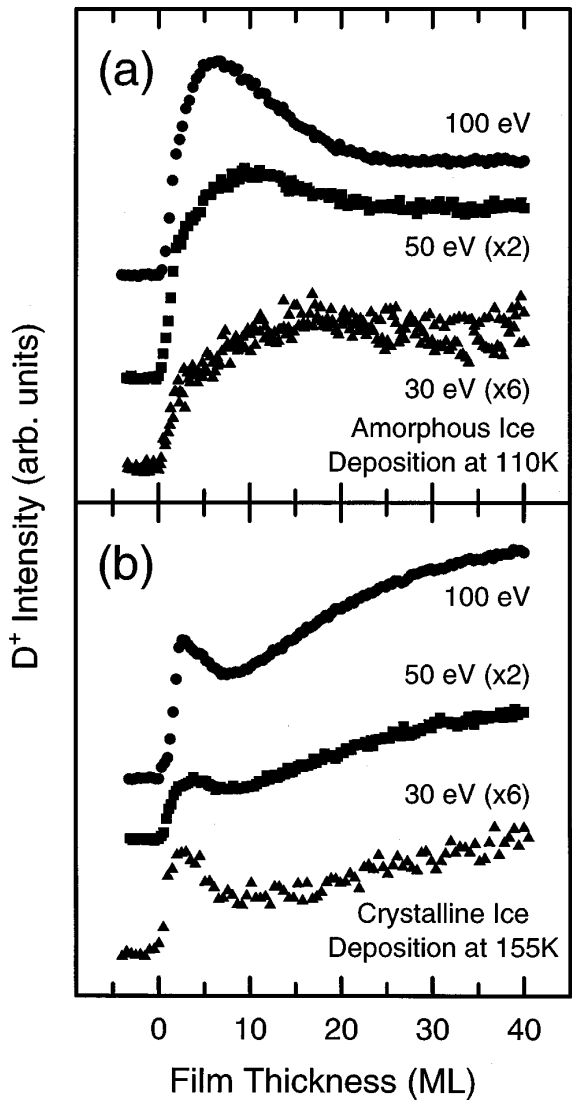

FIG. 7. D^+ ESD yield at selected excitation energies E_i from (a) amorphous and (b) crystalline ice as a function of ice film thickness in ML. The data were acquired during film deposition, and are scaled for display.

crystalline ice shows slow D^+ emission for all coverages, which is expected due to the elevated growth temperature. In Fig. 9 we plot the fast and slow peak heights versus thickness for both ice polymorphs. It is clear that the peak in total yield at low coverage from amorphous ice is due to the presence of the slow component. This serves to explain the difference between the deposition curves at 30, 50, and 100 eV, since the fast/slow ratio is dependent upon E_i. The minimum at $\sim$8 ML on crystalline ice is visible only in the fast component; the slow component rises to a saturation value, and remains constant for thicknesses greater than 2 ML. It is difficult to interpret the data from the crystalline ice, as the sample is warm during deposition and the observed slow component may be present simply because of the surface temperature. It is clear, however, that the fast and slow dissociation cross sections are affected differently by the thickness of the ice layer.

The different behavior of the fast and slow components is unlikely to result from a hot-electron transfer process from the substrate or a backscattering contribution,[51] which would

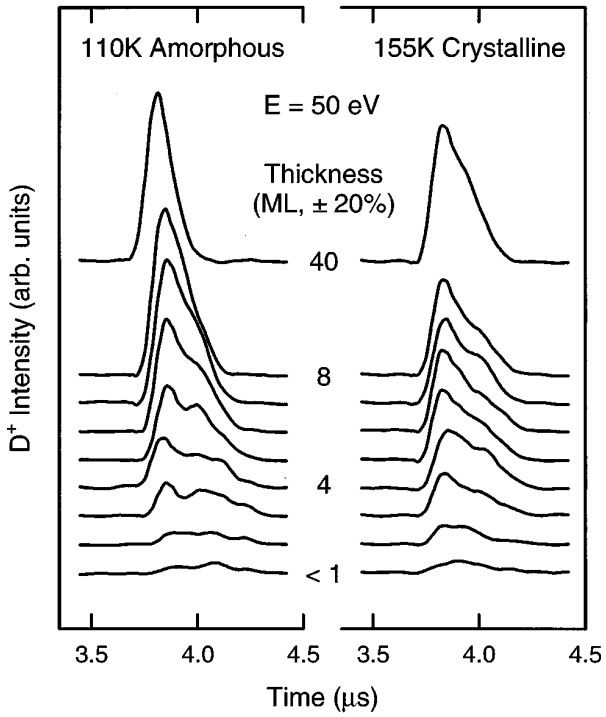

FIG. 8. D^+ time-of-flight distributions at $E_i = 50$ eV as a function of ice thickness for deposition temperatures at 110 (amorphous ice) and 155 K (crystalline ice).

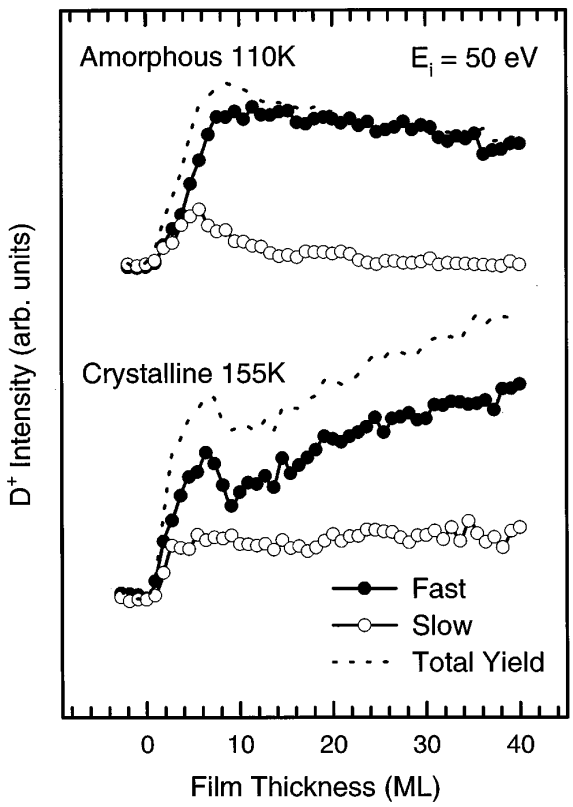

FIG. 9. Fast (filled circles) and slow (empty circles) D^+ time-of-flight peak heights as a function of film thickness at $E_i = 50$ eV. Top: amorphous ice; bottom: crystalline ice.

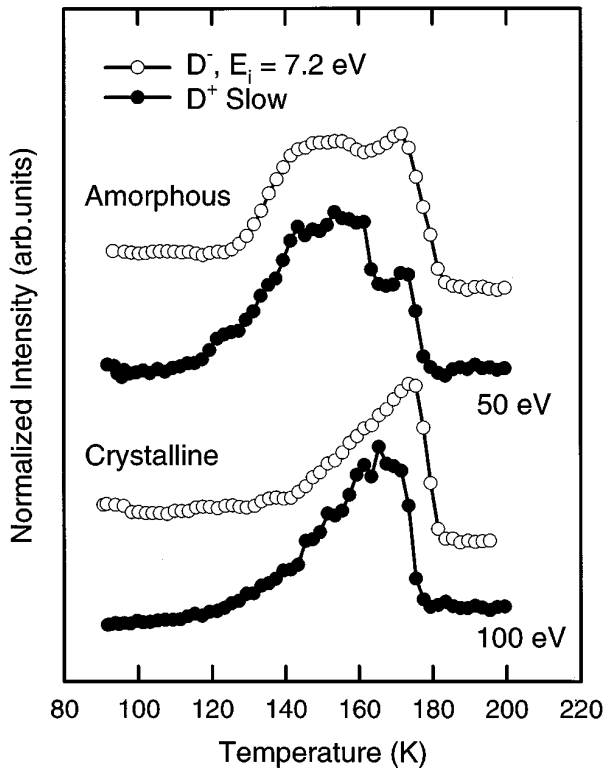

FIG. 10. Comparison of the D^- ESD total yield and the D^+ slow component yield at selected E_i from amorphous (top) and crystalline (bottom) ice as a function of substrate temperature. The data have been normalized for display.

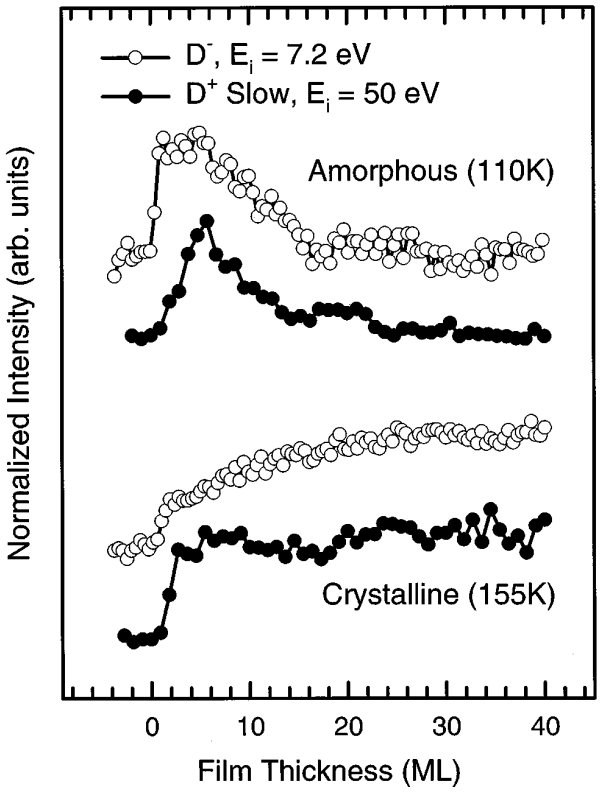

FIG. 11. Comparison of the D^- ESD total yield and the D^+ slow component yield as a function of film thickness for amorphous (top) and crystalline (bottom) ice. The data have been normalized for display.

be expected to affect both decay channels equally. It seems more likely that the thickness dependence is due either to stabilization of a predissociative excited state via interaction with its image charge or to changes in the surface structure with coverage. The different behavior of amorphous and crystalline films disfavors an interaction involving stabilization of a predissociative excited state via image charge interaction. However, a change in the structural environment of surface water molecules can be expected to impact the dissociative excited states affecting the fast and slow deuterons differently. Therefore, we suggest that thickness-dependent changes in the surface structure or morphology of the ice film causes the observed variation of D^+ emission with film thickness.

D. Comparison with negative ion yield and work-function measurements

We have extended our observations to D^- ESD, whose details will be reported in separate publications.[36] These investigations reveal that the thickness and temperature dependence of the D^- total yield is very similar to the slow D^+ yield. In Figs. 10 and 11, the slow D^+ channel peak height and the D^- total yield are plotted as a function of temperature and film thickness, respectively. The curves are surprisingly similar, considering that very different physical processes are responsible for the desorption. However, the ion yields are clearly related, and are being affected similarly by the temperature and thickness dependent changes in the ice.

Figure 12 compares the D^+ fast peak height versus temperature with the work function data of Ref. 8. The work-function measurements were taken on H_2O multilayers deposited on Pt(111), so a shift of $+5$ K was added to the temperature axis to correct for isotope effects[25] for comparison with our D_2O/Pt(111) results. The similarity here is also striking. The orientation of water molecules in the surface

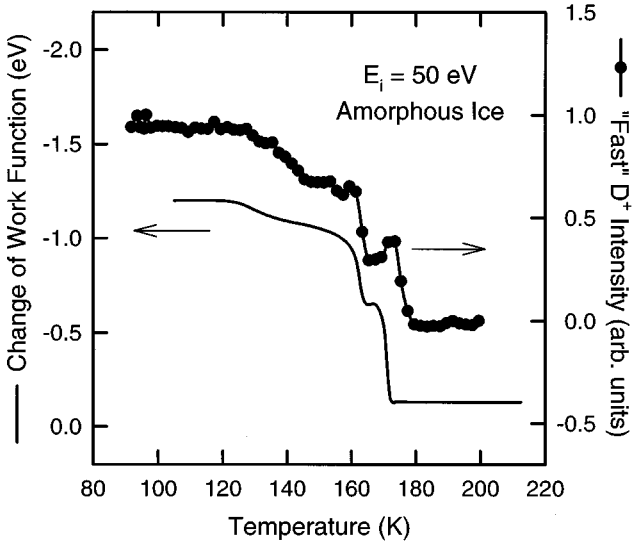

FIG. 12. Comparison of the ice work function [relative to the Pt(111) substrate, left axis] and the D^+ fast component peak height at $E_i = 50$ eV (right axis) vs temperature. The work-function data are taken from Ref. 8.

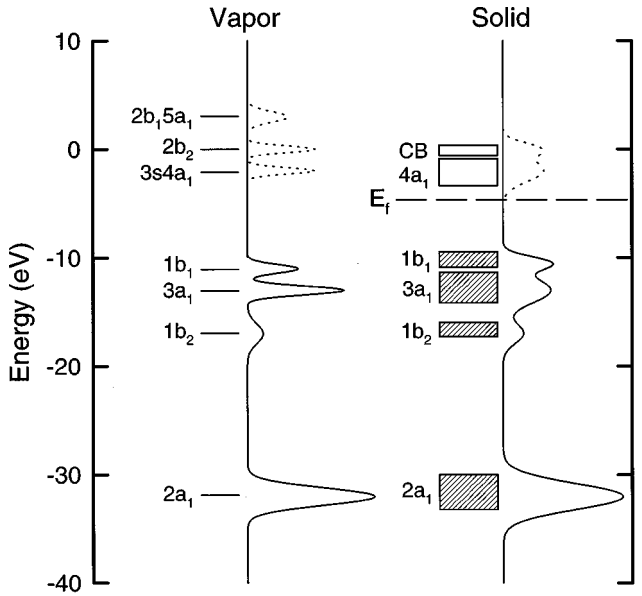

FIG. 13. Schematic diagrams of the electronic structure of the free water molecule (left) and solid water ice (right). Solid lines represent the occupied density of states, and dashed lines represent the density of unoccupied states. The energy scale is referenced to the vacuum level.

dipole layer collectively contributes to the work function. As the surface dipole orientations change, some fraction of the fast deuteron emitters convert to slow deuteron emitters. This similarity between the fast D^+ desorption data and the work-function data suggests that the observed transitions in the yield with temperature and thickness are linked to transitions in the orientation of surface molecules, and therefore to changes in the surface structure.

IV. DISCUSSION

A. Electronic structure of water and ice

Before we discuss the nature of the dissociative excited states responsible for D^+ desorption, it is instructive to review the electronic structure of water and ice. The ground-state electronic configuration of the isolated water molecule can be written $1a_1^2 2a_1^2 1b_2^2 3a_1^2 1b_1^2$.[52] A schematic rendering of the gas-phase valence energy levels and density of states is given in the left side of Fig. 13. The solid (dashed) curve models the occupied (unoccupied) density of states, estimated from calculations and photoemission data.[7–13,29] The $1a_1$ orbital is almost entirely of O $1s$ character (binding energy $\sim$500 eV), and does not play a role in electronic excitations in our energy range. The tetrahedral real-space orbitals can be represented as a linear combination of the valence molecular orbitals: the $1b_2$ and $2a_1$ orbitals are the primary constituents of the O-H bonds, while the $1b_1$ and $3a_1$ make up the oxygen lone-pair orbitals.[7,52] The four lowest unoccupied molecular orbitals are the $4a_1$, $2b_2$, $2b_1$, and $5a_1$. The $4a_1$ and $5a_1$ orbitals are strongly antibonding—occupation of these states leads to breaking of the O-H bond.[40] The $4a_1$ orbital mixes with the $3s$ Rydberg state in the gas phase, and is sometimes referred to as the $3s4a_1$.

There are only small differences in the electronic structure of the free water molecule and condensed ice, with some broadening and minor shifting of the energy levels (Fig. 13, right).[7–13,40] The molecular orbitals retain much of their gas-phase character, so the peaks in the ice valence-band density of states are usually labeled by the same spectroscopic notation as free water. The conduction band of ice is very narrow, with the band minimum less than 1 eV below the vacuum level.[26,27,29] The Fermi level is estimated to be $\sim$5 eV above the $1b_1$ band maximum.[8] The unoccupied $4a_1$ orbital is in the band gap and has a localized (excitonic) character. In the solid state, the unoccupied molecular orbitals are better described as Frenkel excitons, in which the Coulomb attraction localizes the electron-hole pair on the water molecule. The optical-absorption spectra of ice shows a pronounced peak at $\sim$8.3 eV, corresponding to a $1b_1 \rightarrow 4a_1$ transition, well below the photoelectric threshold.[11,12,27] The $4a_1$ state is spatially extended, and should be sensitive to the local bonding environment of the water molecule. The a_1 orbitals are the most perturbed by hydrogen bonding, broadening considerably in the solid state.[7,40] Calculations of ice band structure indicate that the a_1 bands also have the most dispersion, while the $1b_1$ and $1b_2$ bands are virtually dispersionless.[29] One would then expect that electronic excitations involving the a_1 bands would be the most sensitive to changes in the hydrogen bonding environment. Specifically, a reduction of the bandwidth should occur if the hydrogen bonding is weakened, and the lifetimes of electrons and holes in these bands should increase as a consequence.

B. Dissociative excitations of water and ice

There are many excited states of the water molecule which can lead to D^+ emission.[38,40] Ramaker discussed the dissociative excitations of water in the solid and gas phase at length.[40] Table I lists the relevant electronic excitations, their threshold energies, and the ion kinetic energies for D^+ and D^- ESD. The threshold energies for the excitations listed in Table I should be taken as approximate values, since surface

TABLE I. Excitations of water leading to ion emission.

Ref.	Excitation energy (eV)	Valence configuration	Product	Kinetic energy (eV)
40	21–25	$3a_1^{-1}1b_1^{-1}4a_1^1$	D^+	0–4
40	26–31	$1b_1^{-2}4a_1^1$	D^+	4–7
40	31–36	$3a_1^{-2}4a_1^1$	D^+	1–4
	$\sim$70	$2a_1^{-2}$	D^+	$>$7
35,36	$\sim$7	$1b_1^{-1}4a_1^2$	D^-	$<$1

water molecules may have excited state energies which are shifted from gas phase or bulk values. The primary D^+ desorption channels in ice have been assigned to the $3a_1^{-1}1b_1^{-1}4a_1^1$ excited state, which dissociates to 0–4 eV (''slow'') protons, and the $1b_1^{-2}4a_1^1$ excited state, which produces 4–7-eV (''fast'') protons.[40] These are $2h1e$ states, with two holes in the valence band and one electron in the $4a_1$, and their threshold energies are in good agreement with our observed onset for D^+ emission (threshold *A* in Fig. 1). Hydrogen bonding apparently reduces the lifetime of the $3a_1^{-2}4a_1^1$ state to the extent that it does not normally contribute to the desorption process. A H_2O^{2+} two-hole ($2h$) state has been reported in gas phase experiments with a threshold of ~39 eV, which is near threshold *B* in Fig. 1.[49] This state dissociates via Coulomb explosion and is expected to produce protons with kinetic energy >4 eV (''fast''). Since we do not observe any large increase in the fast D^+ intensity as the excitation energy crosses threshold *B*, the H_2O^{2+}-excited states are probably short lived in the solid, and recapture an electron to form $2hle$ states. The emission of very fast deuterons for $E_i > 70$ eV, we tentatively assign to the $2a_1^{-2}$ two-hole state, which has a threshold of 60–70 eV.

While there are many excited states of the water molecule which can lead to positive ion emission, the first negative ion resonance ($^2B_1$) that produces D has the $1b_1^{-1}4a_1^2$ one-hole–two-electron ($1h2e$) configuration, with an excitation energy of about 7 eV.[35,36] The D^+ and D^- ESD products in our experiments do not result from a common neutral parent state, since the excitation energies are different [7 eV for the D^- ($^2B_1$) resonance, versus a threshold of >20 eV for D^+ emission].

Thus, summarizing the relevant electronic excitations, we contend that the slow D^+ results from the $3a_1^{-1}1b_1^{-1}4a_1^1$ and/or $3a_1^{-2}4a_1^1$ configuration, the fast D^+ is produced by the $1b_1^{-2}4a_1^1$ state, and the negative ions are due to the $1b_1^{-1}4a_1^2$ resonance. All of these excitations involve an electron in the $4a_1$ band so the excited states are somewhat similar.

C. Factors influencing ESD yields

The ''slow'' $3a_1^{-1}1b_1^{-1}4a_1^1$ and $3a_1^{-2}4a_1^1$ channels are relatively inoperative below $T_{A1}(T_{C1})$ on the thick amorphous (crystalline) ice surface. Instead, the D^+ desorption at low temperature is dominated by the ''fast'' $1b_1^{-2}4a_1^1$ channel. As the temperature increases, the $3a_1^{-1}1b_1^{-1}4a_1^1$ and $3a_1^{-2}4a_1^1$ begin to contribute more to the yield, at the expense of the $1b_1^{-2}4a_1^1$. The fact that the increase in the slow channel is accompanied by a decrease in the fast channel suggests a population effect; excitations which would normally decay into fast deuterons are instead producing slow deuterons at higher temperature. Physical processes which could produce such an effect include (1) collisions of the outgoing D^+ which reduce its kinetic energy or create secondary ions, or ion survival effects; (2) an ''initial-state'' cross-section change, in which the probability of exciting the $3a_1^{-1}1b_1^{-1}4a_1^1$ or $3a_1^{-2}4a_1^1$ configurations upon electron impact increases, while the probability of exciting the $1b_1^{-2}4a_1^1$ decreases; and (3) a curve crossing from $3a_1^{-1}1b_1^{-1}4a_1^1$ to $1b_1^{-2}4a_1^1$ which ''turns off'' at higher temperatures, due to a temperature-dependent change in the excited-state lifetimes.

1. Ion survival effects

An inelastic scattering process which converts fast D^+ into slow D^+ at high temperature is improbable, as it does not explain the similarity between the D^+ and D^- temperature dependencies, or the thickness-dependent data. However, a change in the ion take-off angle could affect the escape probability, and therefore the total yield. Akbulut, Ma and Madey reported that the H^+ ion angular distribution from H_2O ice narrows considerably as the surface is heated,[47] which can be attributed to reorientation of surface water molecules to point dangling H atoms into the vacuum. It is difficult, however, to explain the details of the thickness and temperature dependence of the velocity-resolved D^+ channels, and the correlation between the slow D^+ and D^- yields, with only a reorientation mechanism. Surface reorientation and the resulting modification to the escape probability probably do contribute to the total yield, but other mechanisms must be invoked to explain the very different behavior of the velocity-resolved D^+ yields.

2. Excitation cross-section effects

It is possible that changes in the orientation and bonding of surface water molecules could be reflected in the total excitation cross section or the branching ratio between the possible excited states. Certainly the cross section for electron-impact excitation of water molecules depends upon the angle of incidence, as the water molecule is not spherically symmetric. However, such a mechanism also fails to explain the similarity between the slow D^+ and D^- data; there is no reason *a priori* to expect that the geometric configurations which increase the probability of exciting the slow D^+ states should also increase the cross section for the negative ion resonance.

3. Changes in excited-state lifetimes

We therefore favor the third process: a curve crossing from the $3a_1^{-1}1b_1^{-1}4a_1^1$ state to the $1b_1^{-2}4a_1^1$ which is reduced at higher temperatures. The potential-energy surfaces for the dissociating water molecule are very complex, and little has been reported on the effect of the solid-state environment on excited-state curve crossings. There are, however, gas-phase calculations which indicate that a $3a_1^{-1}1b_1^{-1}4a_1^1 \rightarrow 1b_1^{-2}4a_1^1$ curve crossing exists,[40] suggesting that such a process can indeed occur on the surface of ice. One possible explanation for the temperature dependence of the curve crossing involves the lifetime of the hole in the $3a_1$ level. The excited-state curve crossing represents the transfer of a hole from the $3a_1$ level to the $1b_1$; an increase in the $3a_1$ hole lifetime would reduce the curve-crossing rate, increase the slow D^+ yield, and decrease the fast D^+ yield, as we observe. Since the ESD yield depends exponentially on the excited-state lifetime,[33] it does not take a large change to affect the yield. A good candidate explanation for the fast/slow temperature dependence, then, involves the lifetime of holes in the $3a_1$ level. In addition, the

yield from the $2a_1^{-2}$ channel above $E_i = 70$ eV increases at high temperature, in a manner similar to the slow D^+ channel. This can be explained if the forces acting to increase the $3a_1$ hole lifetime are also affecting the $2a_1$ hole lifetime. The close similarity between the negative ion yield and the slow positive ion yield leads us to believe that $4a_1$ level is also being perturbed at higher temperatures. An increase in lifetime of the electrons in the $4a_1$ level increases the dissociation probability, and the resulting D^- yield, which would explain our observations.

D. H-bond breakage and excited-state lifetimes

The data are consistent with a temperature dependence of the electron and hole lifetimes in the valence a_1 bands. Since the a_1 bands are sensitive to hydrogen bonding, it seems reasonable that the surface H-bond network is being modified as the ice is heated. A reduction in H bonding is expected to narrow (and possibly shift) the a_1 bands, with a corresponding increase in the lifetime of electrons and holes in these bands. We therefore attribute the observed temperature dependence of the D^+ yield as arising from a reduction in the coordination of surface water molecules beginning at T_{A1} on amorphous ice and T_{C1} on crystalline ice. The reduced hydrogen bonding narrows the a_1 bands, and increases the lifetimes of the $3a_1^{-1}1b_1^{-1}4a_1^1$, $3a_1^{-2}4a_1^1$, $2a_1^{-2}$, and $1b_1^{-1}4a_1^2$ states. These electronic configurations give rise to slow D^+, slow D^+, fast D^+ (for $E_i > 70$ eV) and D^-, respectively. The negative ions and slow deuterons from the low-coverage surface can arise from low-coordination water molecules, which are expected to be populous at low coverage. Surface molecule orientation changes associated with the bond breaking should also result in a change in the work function, which would explain the apparent similarity between the fast ion yield and work function. Temperature-induced hydrogen bond breakage and surface geometry changes, followed by narrowing of the a_1 bands, explain all of the salient features of our data, but further study is still needed to confirm or repudiate some assumptions, such as the $3a_1^{-1}1b_1^{-1}4a_1^1 \rightarrow 1b_1^{-2}4a_1^1$ curve crossing. This explanation, however, is not without precedent: a similar mechanism involving molecular coordination-dependent broadening of the $4a_1$ orbital has been invoked to explain features in the PSD of H^+ from ice at photon energies above the O $1s$ core level.[41]

The process by which H bonds begin to break may be unique to the surface, or may be related to transitions in the bulk ice. A change in the heat capacity and excess entropy has been observed near 125 K for amorphous ice, and near 140 K for crystalline ice, which has been assigned to a configurational change in the bulk.[6,53,54] The physical origin of this ''glass transition'' is still a topic of debate. In a recent paper, Dosch, Lied, and Pilgram invoked activated migration of L defects in the near-surface layer to explain their x-ray scattering measurements of the disruption of surface H bonds and surface premelting on hexagonal ice at atmospheric pressure.[19] An L defect can be thought of as a H-bond vacancy. Migration of these L defects to the surface can result in the rupturing of surface H bonds, and can produce the coordination-dependent excited-state lifetime effects we observe. The activated migration of pre-existing L defects at 120 K has also been implicated in depolarization thermocurrent measurements in ice.[55] Our bond-breaking model is consistent with these earlier observations, and the activated migration of L defects provides a mechanism for the reduction in surface coordination. Since the cross section for desorption is rather large, a surface defect density of $\sim 10^{12}$ cm^{-2} or a bulk defect density of $\sim 10^{18}$ cm^{-3} is required to explain our yields. Measurements of the Bjerrum defect concentration in vapor-deposited ice have not been reported, to our knowledge, but Dosch, Lied, and Pilgram reported defect densities of $\sim 10^{19}$ cm^{-3} in the near surface region of bulk ice samples.[19] The proposed H-bond breaking which leads to changes in the excited-state lifetimes is, therefore, consistent with a surface manifestation of bulk ice transitions.

V. CONCLUSION

The electron-stimulated desorption of deuterium ions from D_2O ice has been found to be very sensitive to the surface hydrogen-bonding environment and film morphology. Our analysis of the data suggests that water molecules at the ice surface undergo a reduction in hydrogen bonding near 120 K (135 K) on amorphous (crystalline) ice, well below the temperature at which the film desorption rate becomes appreciable. This reduction in coordination number may be related to thermally-activated migration of Bjerrum L defects to the surface. By 140 K the amorphous surface has reached a stable configuration in which the H-bond coordination number does not change, and near 162 K the ice crystallizes. Our observations of the total yield, time-of-flight distributions, and the thickness dependence of the D^+ desorption can be explained by a narrowing of the a_1 valence bands caused by a reduction in hydrogen bonding, which increases the lifetime of electrons and holes in these bands. The similarities between the temperature and thickness dependence of the D^+ yield, D^- yield, and work function give further evidence of temperature-dependent changes in the surface structure. We contend that the slow D^+ results from the $3a_1^{-1}1b_1^{-1}4a_1^1$ and $3a_1^{-2}4a_1^1$ configurations, the fast D^+ is produced by the $1b_1^{-2}4a_1^1$ state, and the negative ions are due to the $1b_1^{-1}4a_1^2$ resonance. We have also seen evidence of a threshold at ~ 70 eV producing fast ions, which we have assigned to the $2a_1^{-2}$ state. These results imply that the local environment of a water molecule is important for its dissociation cross section, and such structure-dependent effects may be important for ice and water radiolysis in astrophysics, biophysics, and atmospheric chemistry.

Note added in proof. A recalibration revealed that the temperatures quoted should be modified by $T_{\text{new}} = 0.91 T_{\text{old}} + 10$ K. This recalibration does not change any of the conclusions.

ACKNOWLEDGMENTS

The authors would like to thank B. D. Kay, G. A. Kimmel, R. S. Smith, B. Rowland, S. A. Joyce, and T. E. Madey (Rutgers) for helpful discussions. This work was supported by the U.S. Department of Energy, Office of Basic Energy Sciences. Pacific Northwest National Laboratory is operated for the U.S. Department of Energy by Battelle Memorial Institute under Contract No. DE-AC06-76RLO 1830.

*Corresponding author: T. M. Orlando, telephone 509-376-9420; fax: 509-376-6066; electronic address: tm_orlando@pnl.gov

[1] See, for example, R. E. Johnson, Rev. Mod. Phys. **68**, 305 (1996); W. L. Brown, W. M. Augustyniak, L. J. Lanzerotti, R. E. Johnson, and R. Evatt, Phys. Rev. Lett. **45**, 1632 (1980); M. S. Westley, R. A. Baragiola, R. E. Johnson, and G. A. Baratta, Nature (London) **373**, 405 (1995); W. L. Brown, L. J. Lanzerotti, and R. E. Johnson, Science **218**, 525 (1982); C. Y. R. Wu, B. W. Yang, and D. L. Judge, Planet. Space Sci. **42**, 273 (1994).

[2] See, for example, W. Wang, M. Yan, D. Becker, and M. D. Sevilla, Radiat. Res. **137**, 2 (1994); S. G. Swarts, M. D. Sevilla, D. Becker, C. J. Tokar, and K. T. Wheeler, *ibid.* **129**, 333 (1992).

[3] H.-G. Heide, Ultramicroscopy **14**, 271 (1984); C. T. Reimann, J. W. Boring, R. E. Johnson, J. W. Garrett, K. R. Farmer, W. L. Brown, K. J. Marcantonio, and W. M. Augustyniak, Surf. Sci. **147**, 227 (1984).

[4] See, for example, R. Feder and J. B. Pendry, Solid State Commun. **26**, 519 (1978); H. J. Fitting, Phys. Status Solidi A **26**, 525 (1974).

[5] G. A. Kimmel and T. M. Orlando, Phys. Rev. Lett. **75**, 2606 (1995).

[6] M. G. Sceats and S. A. Rice, in *Water, A Comprehensive Treatise*, edited by F. Franks (University of Cambridge, Cambridge, 1982), p. 83.

[7] P. A. Thiel and T. E. Madey, Surf. Sci. Rep. **7**, 211 (1987).

[8] E. Langenbach, A. Spitzer, and H. Luth, Surf. Sci. **147**, 179 (1984).

[9] B. Baron, D. Hoover, and F. Williams, J. Chem. Phys. **68**, 1997 (1978); M. U. Sander, K. Luther, and J. Troe, Ber. Bunsenges. Phys. Chem. **97**, 953 (1993).

[10] G. B. Fisher (unpublished); M. J. Campbell, L. Liesengang, J. D. Riley, R. C. G. Leckey, J. G. Jenkin, and R. T. Poole, J. Electron Spectrosc. Relat. Phenom. **15**, 83 (1979).

[11] T. Shibaguchi, H. Onuki, and R. Onaka, J. Phys. Soc. Jpn. **42**, 152 (1977).

[12] R. Onaka and T. Takahashi, J. Phys. Soc. Jpn. **24**, 548 (1968).

[13] B. Baron and F. Williams, J. Chem. Phys. **64**, 3896 (1976).

[14] R. L. Hudson and M. H. Moore, J. Phys. Chem. **96**, 6500 (1992); J. E. Schaff and J. T. Roberts, *ibid.* **98**, 6900 (1994); L. Delzeit, M. S. Devlin, B. Rowland, and J. P. Devlin, *ibid.* **100**, 10 076 (1996).

[15] V. Buch, L. Delzeit, C. Blackledge, and J. P. Devlin, J. Phys. Chem. **100**, 3732 (1996); J. P. Devlin and V. Buch, *ibid.* **99**, 16 534 (1995).

[16] U. Starke, N. Materer, A. Barbieri, R. Doll, K. Heinz, M. A. Van Hove, and G. A. Somorjai, Surf. Sci. **287**, 432 (1993); N. Materer, U. Starke, A. Barbieri, M. A. Van Hove, G. A. Somorjai, G.-J. Kroes, and C. Minot, J. Phys. Chem. **99**, 6267 (1995).

[17] P. Jenniskens and D. F. Blake, Science **265**, 753 (1994).

[18] M. F. Toney, J. N. Howard, J. Richer, G. L. Borges, J. G. Gordon, O. R. Melroy, D. G. Wiesler, D. Yee, and L. B. Sorensen, Nature (London) **368**, 444 (1994); A. Lied, H. Dosch, and J. H. Bilgram, Phys. Rev. Lett. **72**, 3554 (1994); H. Dosch, A. Lied, and J. H. Bilgram, Surf. Sci. **327**, 145 (1995).

[19] H. Dosch, A. Lied, and J. H. Bilgram, Surf. Sci. **366**, 43 (1996).

[20] N. J. Sack and R. A. Baragiola, Phys. Rev. B **48**, 9973 (1993).

[21] R. Pletzer and E. Mayer, J. Chem. Phys. **90**, 5207 (1989).

[22] D. E. Brown, S. M. George, C. Huang, E. K. L. Wong, R. B. Rider, R. S. Smith, and B. D. Kay, J. Phys. Chem. **100**, 4988 (1996).

[23] G. B. Fisher and J. L. Gland, Surf. Sci. **94**, 446 (1980).

[24] R. S. Smith, C. Huang, E. K. L. Wong, and B. D. Kay, Surf. Sci. Lett. **367**, L13 (1996).

[25] R. J. Speedy, P. G. Debenedetti, R. S. Smith, C. Huang, and B. D. Kay, J. Chem. Phys. **105**, 240 (1996).

[26] M. Michaud, P. Cloutier, and L. Sanche, Phys. Rev. A **44**, 5624 (1991); H. Ibach and S. Lehwald, Surf. Sci. **91**, 187 (1980).

[27] K. Kobayashi, J. Phys. Chem. **87**, 4317 (1983).

[28] M. Morgenstern, T. Michely, and G. Comsa, Phys. Rev. Lett. **77**, 704 (1996); M. Morgenstern, J. Muller, T. Michely, and G. Comsa, Z. Phys. Chem. (Munich) (to be published).

[29] V. F. Petrenko and I. A. Ryzhkin, Phys. Rev. Lett. **71**, 2626 (1993); G. P. Parravicini and L. Resca, Phys. Rev. B **8**, 3009 (1973).

[30] V. P. Dmitriev, S. B. Rochal, and P. Toledano, Phys. Rev. Lett. **71**, 553 (1993).

[31] U. Essmann and A. Geiger, J. Chem. Phys. **103**, 4678 (1995).

[32] For an extensive review and comprehensive bibliography, see, V. F. Petrenko, U.S. Army Corps of Engineers Cold Regions Research & Engineering Laboratory, *Electrical Properties of Ice*, Special Report No. 93-20 (unpublished) (1993), and other booklets in the series.

[33] Reviews of ESD and PSD include R. D. Ramsier and J. T. Yates, Jr., Surf. Sci. Rep. **12**, 243 (1991); P. Avouris and R. E. Walkup, Annu. Rev. Phys. Chem. **40**, 173 (1989); T. E. Madey, D. E. Ramaker, and R. Stockbauer, *ibid.* **35**, 215 (1984).

[34] G. A. Kimmel, T. M. Orlando, C. Vezina, and L. Sanche, J. Chem. Phys. **101**, 3282 (1994); G. A. Kimmel, R. G. Tonkyn, and T. M. Orlando, Nucl. Instrum. Methods Phys. Res. B **101**, 179 (1995); G. A. Kimmel and T. M. Orlando, Phys. Rev. Lett. **77**, 3983 (1996).

[35] P. Rowntree, L. Parenteau, and L. Sanche, J. Chem. Phys. **94**, 8570 (1991); M. Tronc, R. Azria, Y. Le Coat, and E. Illenberger, J. Phys. Chem. **10**, 14 745 (1996).

[36] W. C. Simpson, M. T. Sieger, L. Parenteau, L. Sanche, and T. M. Orlando (unpublished); W. C. Simpson, L. Parenteau, R. S. Smith, L. Sanche, and T. M. Orlando, Surf. Sci. (to be published).

[37] T. E. Madey and J. T. Yates, Chem. Phys. Lett. **51**, 77 (1977).

[38] J. O. Noell, C. F. Melius, and R. H. Stulen, Surf. Sci. **157**, 119 (1985).

[39] S. L. Bennett, C. L. Greenwood, E. M. Williams, and J. L. de Segovia, Surf. Sci. **251/252**, 857 (1991).

[40] D. E. Ramaker, Chem. Phys. **80**, 183 (1983).

[41] R. A. Rosenberg, P. R. LaRoe, V. Rehn, J. Stohr, R. Jaeger, and C. C. Parks, Phys. Rev. B **28**, 3026 (1983).

[42] M. Q. Ding, E. M. Williams, J. P. Adrados, and J. L. de Segovia, Surf. Sci. Lett. **140**, L264 (1984).

[43] E. Bertel, D. E. Ramaker, R. L. Kurtz, R. Stockbauer, and T. E. Madey, Phys. Rev. B **31**, 6840 (1985).

[44] R. Stockbauer, D. M. Hanson, S. A. Flodstrom, and T. E. Madey, Phys. Rev. B **26**, 1885 (1982).

[45] D. Coulman, A. Puschmann, U. Hofer, H.-P. Steinruck, W. Wurth, P. Feulner, and D. Menzel, J. Chem. Phys. **93**, 58 (1990).

[46] R. H. Stulen and R. A. Rosenberg, J. Vac. Sci. Technol. A **2**, 1051 (1985); R. A. Rosenberg, V. Rehn, V. O. Jones, A. K. Green, C. C. Parks, G. Loubriel, and R. H. Stulen, Chem. Phys. Lett. **80**, 488 (1981).

[47] M. Akbulut, Z. Ma, and T. E. Madey (unpublished).

[48] J. A. Ghormley, J. Chem. Phys. **46**, 1321 (1967); **48**, 503 (1968); B. S. Berland, D. E. Brown, M. A. Tolbert, and S. M. George,

Geophys. Res. Lett. **22**, 3493 (1995).
[49] P. J. Richardson, J. H. D. Eland, P. G. Fournier, and D. L. Cooper, J. Chem. Phys. **84**, 3189 (1986).
[50] M. T. Sieger and T. M. Orlando, Surf. Sci. (to be published).
[51] M. Michaud and L. Sanche, Phys. Rev. A **36**, 4672 (1987).
[52] I. N. Levine, *Quantum Chemistry*, 4th ed. (Prentice-Hall, Englewood Cliffs, NJ, 1991), p. 468; C. R. Claydon, G. A. Segal, and H. S. Taylor, J. Chem. Phys. **54**, 3799 (1971).
[53] G. P. Johari, Philos. Mag. **35**, 1077 (1977); J. Chem. Phys. **95**, 2955 (1991); **102**, 6224 (1995); G. P. Johari, A. Hallbrucker, and E. Mayer, *ibid.* **92**, 6742 (1990); A. Hallbrucker and E. Mayer, J. Phys. Chem. **93**, 7751 (1989).
[54] M. Fisher and J. P. Devlin, J. Phys. Chem. **99**, 11 584 (1995).
[55] G. P. Johari and S. J. Jones, J. Chem. Phys. **62**, 4213 (1975).